Predicting Creep Behaviour in the Historical Valkenburg Calcarenite Mines Using LSTM Neural Networks

Nikolaos Antoniadis[1], Wout Broere[2], Guillaume Rongier[3] & Dominique Ngan-Tillard[4]

[1]PhD Candidate, School of Mining & Metallurgical Engineering, National Technical University of Athens, Athens, Greece, email: nikolaosantoniadis@metal.ntua.gr

[2]Associate Professor, Faculty of Civil Engineering and Geosciences, Delft University of Technology, Delft, The Netherlands, email: W.Broere@tudelft.nl

[3]Assistant Professor, Faculty of Civil Engineering and Geosciences, Delft University of Technology, Delft, The Netherlands, email: G.Rongier@tudelft.nl

[4]Associate Professor, Faculty of Civil Engineering and Geosciences, Delft University of Technology, Delft, The Netherlands, email:D.Ngan-Tillard@tudelft.nl

ABSTRACT

The Valkenburg calcarenite mines in the Netherlands, dating back to the 15th century, represent an important historical monument. Initially, the mines were exploited using the room-and-pillar method, and nowadays serve as a tourist attraction. Throughout the years, these mines have suffered structural instabilities due to unregulated extraction practices and the inherent soft nature of the calcarenite ($\sigma_{ci} \simeq$ 2.5 MPa). This study focuses on investigating the long-term creep behaviour of mine pillars using a dataset collected from an advanced fibre optic monitoring system, covering four years of continuous observations across 81 pillars. Traditional geospatial and statistical analysis results provided weak correlations and conflicting results between stability indicators (pillar height, effective width, and overburden thickness) and the observed deformation trends, necessitating a more advanced approach. To address this, Long Short-Term Memory (LSTM) neural networks were employed to predict pillar deformation and assess long-term stability risks. The LSTM models successfully captured the complex, non-linear deformation patterns of the mine pillars, accurately predicting deformation values up to approximately 150 days, after which deviations from the observed values occurred. The LSTM models also faced challenges in certain training sets where deformations were associated with pronounced seasonal patterns. The findings highlight the potential of continuous monitoring combined with predictive modelling to improve early warning and preserve the structural integrity of historical underground sites, while ensuring their safe utilisation for future generations.

Keywords: Creep, Fibre Optics, Room and Pillar, Calcarenite, Machine Learning, LSTM

INTRODUCTION

The limestone mines located in Valkenburg, Limburg, the Netherlands, have been exploited since the 16th century for the use of building materials. Houses in Valkenburg and the surrounding area used to be built partly or entirely from these building blocks. The mines' corridor system extends multiple kilometres underneath the ground surface and is nowadays used as a tourist attraction.

The exploitation method used was the room and pillar method, where the rooms or chambers of the material are excavated, while some pillars of untouched material are left to support the roof and the overburden (Franqueira, 2020). The extraction of the limestone and marl continued until about 1950, but it was never regulated. The uncontrolled and irregular exploitation patterns, the superimposed mining levels, as well as the low compressive strength, long-term deterioration, and weathering of the calcarenite formations, have resulted in instability and rapid and major collapses of different parts of the mines. When mines are located close to the surface, their collapse can result in air blasts both inside and outside the mine, surface settlements, and structural problems in nearby buildings.

In some cases, a considerable time period exists between the end of the exploitation and the collapse. Therefore, it is considered that long-term behaviour (creep and deterioration) is impacting the stability of the individual pillars. Moreover, over-mining and pillar “stealing” also affect the stability of the pillars and the mines overall. Other factors, such as climate change, might influence the rate of the process or even the processes involved. For example, in the Fallenberg collapse of 1920, it was reported that three days before the collapse, heavy rainfall had occurred (Bekendam, 1998).

To monitor these deformation phenomena in some mines, such as the Jezuitenberg mine, classic instruments to measure the deformation of the pillars have been installed. Similarly, to measure and assess the stability of the existing pillars, an optical fibre-based monitoring system was installed in October 2019 in the mines of Valkenburggroeve and Sibbergroeve. The purpose of this paper is to investigate the long-term creep behaviour of the calcarenite pillars by using the high-resolution fibre optic monitoring data. To improve deformation predictions and stability assessments, Long Short-Term Memory (LSTM) neural networks are applied to capture complex, time-dependent deformation patterns.

VALKENBURGGROEVE & SIBBERGROEVE MINES

The Valkenburggroeve, also known as Gemeentegrot or Gemeentegroeve, is one of the biggest underground mines in the Province of Limburg, the Netherlands. It has underground passages which extend for more than 50 kilometres. Over the centuries, the Valkenburggroeve has been used for various purposes, including air raid shelters, mushroom farms, a war factory, and a secret church. Another mine located in the Province of Limburg is the Sibbergroeve. This mine has been exploited from the 17th century until today, and part of it is currently used for walking, biking and ATV tours. In the older, eastern part of the quarry, many pillars have deteriorated and exhibit cracks and stability issues. Moreover, in Sibbergroeve, vertical, cylindrical earth pipes are common, and multiple roof collapses can be seen. In both mines, buildings and roads cover the majority of the ground surface above the quarries.

Both mines are excavated in the Maastricht Formation, a Cretaceous era formation, composed of calcarenite. The formation is divided into 6 members, which are separated by hard grounds called “horizons”. The Valkenburggroeve mine is mostly excavated in both the Emael and Nekum members, while the Sibbergroeve mine is excavated in the upper part of the Emael member (Bekendam, 2008). It should be noted that the strength of each calcarenite member differs, depending on its grain composition, fossils and cherts' appearances.(Felder & Bosch, 2000). In general, the calcarenite has a dry compressive strength of 1.5-4 MPa (Bekendam, 1998).

As previously mentioned, the main issue in the mines is the long-term behaviour of the calcarenite (creep and dissolution). Long-term deterioration of the calcareous material, especially at shallow depths, occurs by either the dissolution of cementing bonds or the formation of micro-cracks (Bekendam, 1998; Van Paassen et al., 2008). Creep deformation can eventually lead to spalling of pillars or roof collapse, two of the main failure mechanisms in the room and pillar mines. Low confining stresses and high deviatoric stress in the excavation walls further accelerate the deterioration process. As a consequence of creep deformation, pillars can fail at a stress below their short-term strength. Even many years after excavation, these deformations can cause the pillar to fail and eventually might lead to large-scale collapse (Bekendam, 1998).

(a) (b)

Figure 1. *An hourglass-shaped pillar after the separation of the fracture planes in the Sibbergroeve mine: (a) view from the front side and (b) view from the opposite side. Extensometer O3C-3 is installed in the pillar. Photographs taken by the authors.*

MONITORING SYSTEM

To monitor the long-term deformations that take place in the calcarenite pillars, a novel fully automatic fibre optic system was installed by Fugro in the autumn of 2019 in the Valkenburggroeve and Sibbergroeve mines. The system was placed in areas where (a) deteriorated pillars are located, (b) in pillars next to collapsed areas, or (c) in areas where movements were expected to manifest in the future (Figure 1). The fibre optic sensor was installed by bolting two anchors into the limestone. One was bolted vertically in the ceiling, and one horizontally in the pillar wall, near the floor (Figure 2). Through the system, measurements for the raw wavelength from all sensors every 7 and 30 seconds for the Gemeentegroeve and Sibbergroeve are acquired, respectively. The wavelengths are consequently converted into strain using predetermined calibration parameters, and the temperature sensor is used to correct for thermal effects. The deformations are also acquired by accounting for the sensor's length. Finally, the creep velocity and acceleration are calculated daily by fitting a 1st and 2nd order polynomial to the creep measurements (Noordermeer et al., 2023). The datasets provided by Fugro range over 4 years and for a total of 81 pillars for the two mines. The measurements are all down-sampled and stored in a database.

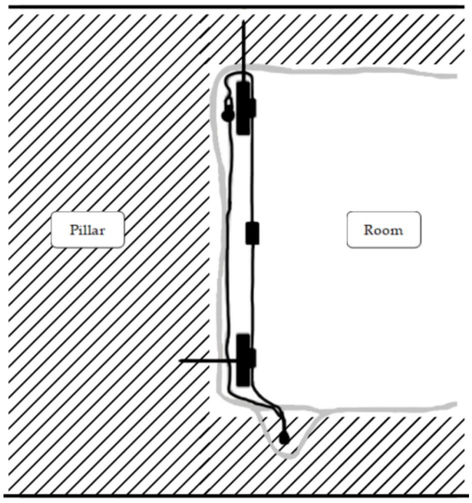

Figure 2. *Sketch of the optic fibre sensor, which is mounted on the limestone pillar wall and ceiling. Figure adapted after Noordermeer et al. (2023), ISRM 2023 Congress Proceedings, © ÖGG.*

By analysing the timeseries, some early patterns are apparent (Figure 3). Natural and non-natural fluctuations can be observed. An example of natural fluctuation would be the "shortening" of the pillar. Unnatural fluctuations are caused by malfunctions in the measuring system, and repair works which are required to resolve these malfunctions. Moreover, in the timeseries, two types of phenomena have been observed: (a) One-off 'jumps' in the creep measurements, which are usually of the order of a few μm. These jumps are mostly related to blocks falling in the surrounding area, either from the roof or from the sides of the pillars. Moreover, 'jumps' or outliers may be caused by unexpected events, such as the Tongan volcanic eruption on 15 January 2022. (b) Temperature variations, which lead to fluctuations in the creep measurements. This effect mainly occurs at the locations near the entrances of the quarries or near shafts through which outside air flows into the underground mine. It should be noted that the strain sensors in the monitoring system are calibrated to compensate for temperature variations.

Two phases can be distinguished in the creep measurements of the monitoring system (Figure 3a). An initial phase from December 2019 until the beginning of 2020, where high creep velocity was observed in all the sensors (Bekendam, 2019). Until the end of 2020, there was an increase in the creep speed per day and the creep speed per month. Noordermeer et al. (2023) hypothesised that the installation of the sensors caused local tension in the limestone rock around the anchors, due to the low strength of the rock (UCS of 1.5–4 MPa). After some time, the creep values started to stabilise and present a less steep increase, while the creep acceleration per month decreased to approximately zero, indicating that the initial period had ended and a second stage, where steady creep takes place, began.

Another assumption for the two phases observed is that the initial startup phase, where a fast increase in creep is observed, is attributed to an ongoing system-related creep. This system-related creep could be attributed to factors such as the tensioning of the fibre optic cables or the galvanisation process, which might induce a consistent, albeit declining, tension in the sensors. Therefore, the initial high creep velocities might represent the combined effects of both the pillar's inherent creep and the gradual relaxation of the measurement system itself. The creep of the system would then still be ongoing throughout the entirety of the system's lifespan, parallel to the pillar's creep.

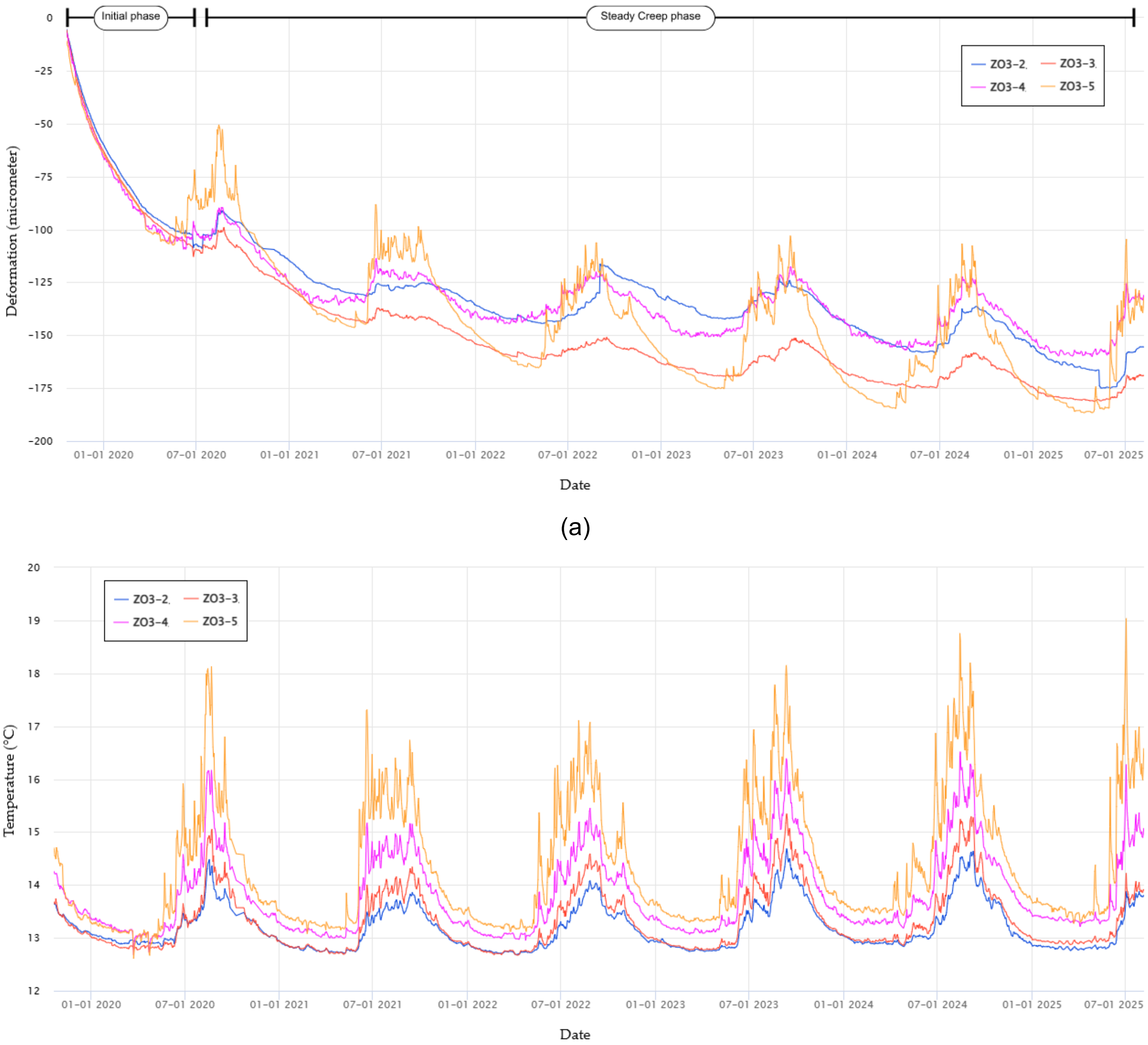

(a)

(b)

Figure 3. *(a) The deformation timeseries, with the two phases denoted and (b) the temperature fluctuations for extensometers ZO3-2, ZO3-3, ZO3-4, and ZO3-5.*

METHODOLOGY

To analyse the extensive dataset, traditional geospatial (tributary area method and pillar dimensions) and statistical analyses (correlation analysis using Pearson and Spearman coefficients) were initially conducted to explore relationships between pillar geometry and deformation trends. However, the results revealed weak correlations between parameters such as pillar height, effective width, and overburden thickness with observed deformation rates. In many cases, the trends were inconsistent or conflicting, indicating that these empirical and bivariate approaches were insufficient for reliably assessing pillar stability.

The application of Long Short-Term Memory (LSTM) neural networks in geotechnical engineering has become increasingly popular due to their ability to model complex temporal dependencies. LSTM networks have demonstrated particular effectiveness in scenarios where traditional methods, such as linear regression or empirical models, are inadequate due to the non-linear and dynamic nature of geotechnical processes (He & Chen, 2023a, 2023b; Seo & Chung, 2022; Xie et al., 2019). For that reason, it was decided to use LSTMs to model the timeseries.

The datasets that were used for training the LSTMs were composed of six (6) variables. These variables were the creep, temperature, and precipitation timeseries (Figure 5), as well as the height, effective width, and overburden thickness of each pillar. The former variables are dynamic, while the latter are static. It was decided to transform the static variables to pseudo-dynamic, giving them a temporal dimension (Leontjeva & Kuzovkin, 2016). The datasets for each pillar containing the selected features were combined into a unified single dataset. The data was then sequentially split into training (70%), validation (10%), and testing sets (20%). The models were trained and predictions were generated for different combinations of sequence lengths (100 and 200) and epochs (50, 80, 100, 200, 500, 1000, and 2000). The LSTM model was defined with specified parameters, including the hidden size (= 50) and the number of layers (= 2). It should be noted that the sequence length in the LSTM model defines the number of previous time steps used as input to predict the subsequent deformation value. In this study, the sequence lengths of 100 and 200 were selected to investigate the influence of short-term versus longer-term temporal dependencies in the creep behaviour of the extensometers. A shorter sequence length (100) focuses on more recent deformation patterns, and it is expected to better capture short-term fluctuations. On the other hand, a longer sequence length (200) improves the representation of long-term trends such as seasonal effects. Moreover, the number of epochs represents the number of complete passes through the training dataset during model optimisation. A range of epochs (50–2000) was tested to evaluate the model's learning behaviour and identify potential underfitting or overfitting. The hidden size of the LSTM determines the number of units in each LSTM layer and thus controls the model's capacity to learn complex temporal relationships. In this case, it was set to 50. A moderate hidden size was selected to capture the non-linear creep behaviour, while avoiding excessive model complexity that would lead to overfitting. Finally, the number of LSTM layers was fixed at 2, enabling the model to learn hierarchical temporal features. Afterwards, predictions were made based on these models, and they were evaluated with several metrics (Mean Absolute Error, Root Mean Squared Error, and R-squared). It is important to note that, due to maintenance work and unexpected events, gaps and outliers were present in the temperature and deformation data. To address these issues, the relevant dates were identified from Fugro's maintenance reports, missing values were interpolated, and outliers were filtered out. For this study, the datasets for extensometers O3D_1 and O3C_1 will be utilized, the locations of which are presented in Figure 4.

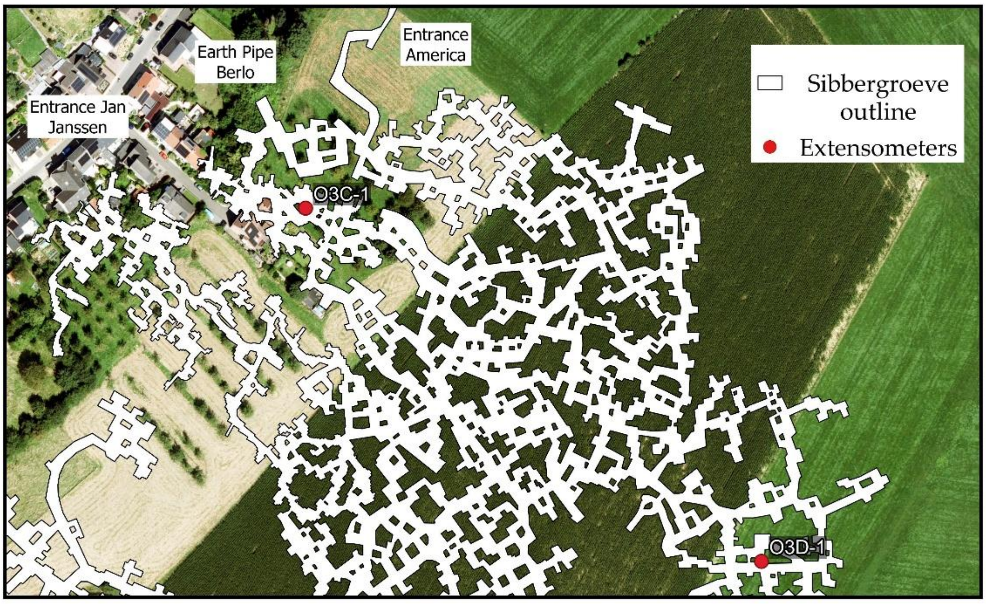

Figure 4. *Location of Extensometer O3D_1 & O3C_1*

(a)

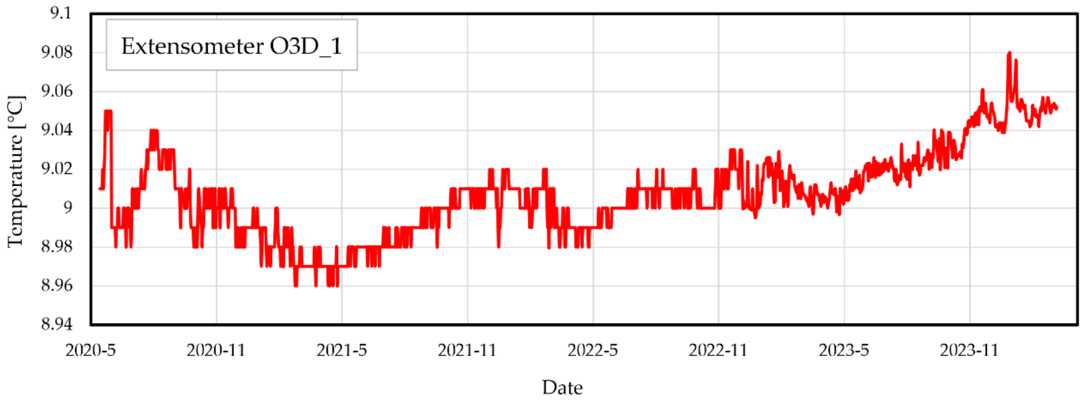

(b)

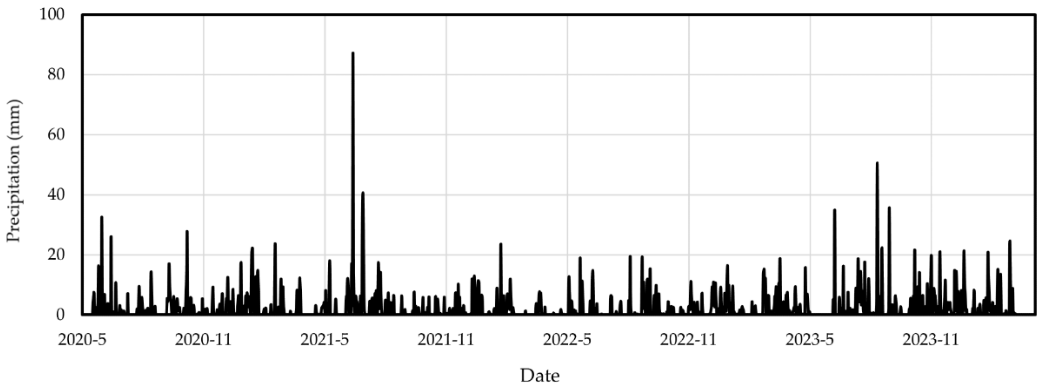

(c)

Figure 5. *Temperature timeseries for extensometer (a) O3D_1 and (b) O3C_1 & (c) Precipitation timeseries*

It should be noted that in Figure 5, a slight but consistent increase in mean temperature is observed over the monitoring period, especially in the extensometer O3C_1. It is not clear where this trend is attributed. The most likely explanation is that it is a combination of factors, such as the broader climatic variations, site-specific conditions such as ventilation patterns within the mine, and the touristic activity. Specifically, the variation in O3C_1 is approximately 0.8 °C, while in O3D_1 it is only 0.12 °C. Such limited temperature changes are negligible and do not influence the observed deformation patterns of the pillars. Moreover, the precipitation data used in this study (Figure 5c) were obtained from the Royal Netherlands Meteorological Institute (KNMI) monitoring network. The closest available station to the study area is the Maastricht weather station, which is representative of regional precipitation patterns affecting the Valkenburggroeve and Sibbergroeve. The dataset consists of hourly measurements that are quality-controlled, corrected, and supplemented where necessary by KNMI.

Concerning the framework that was followed, two approaches were decided when feeding the datasets into the LSTM models. The first approach was based on the assumption that there are two distinguishable phases in the timeseries, as aforementioned. For this approach, the initial phase, related to the installation process, is removed and only the deformation timeseries after that are taken into account. In the second approach, the observed high creep values are considered to be attributed to an ongoing monitoring system-related creep. Therefore, incorporating the initial startup phase into the analysis could offer a more comprehensive understanding of the long-term creep behaviour of the limestone pillars. The second approach was further divided into two procedures. In Procedure A, a logarithmic curve was fitted to the raw data. This curve would represent the contribution of the sensor system's relaxation over time. By subtracting this fitted logarithmic trend from the total observed creep, the residual creep could then be interpreted as the true creep of the limestone pillars, independent of the sensor system's influence. In Procedure B, the raw data from the extensometer, including the initial period, is fed directly into the LSTM without fitting a logarithmic curve. The purpose of this procedure is to inquire whether the LSTM is capable of understanding the underlying logarithmic trends in the timeseries.

It was decided that the dataset from different extensometers would not be combined into a single dataset, so that it would be ensured that the model training process would be tailored to the unique characteristics and behaviour of each extensometer. This would allow it to capture the specific response patterns associated with each one. Consequently, the models were trained and validated separately for each extensometer, with a training range of 1200 days.

The dataset used in this study is available and can be accessed upon request through the Municipality of Valkenburg.

RESULTS

Approach 1 – Removal of the initial start-up phase

During Approach 1, the initial start-up phase is removed. Models for sequence lengths of 100 and 200, across various epochs, were used to predict deformation values. The models' performance metrics for extensometers O3D_1 and O3C_1 are presented in Tables 1 & 2, respectively.

For extensometer O3D_1, the best model for sequence length 100 is achieved at 1000 epochs (RMSE = 3.26 & R^2 = 0.71). Beyond this, performance declines, indicating overfitting. With a sequence length of 200, performance fluctuates, with the best results at 500 epochs (RMSE = 4.22 & R^2 = 0.53). While short-term fluctuations are captured, the seasonal downward trend is not, and longer sequences reduce accuracy (Figure 6a). On the other hand, the results for the extensometer O3C_1 show a different picture. The best model for sequence length 100 is at 500 epochs (RMSE = 0.53 & R^2 = 0.98), while sequence length 200 achieves best performance at 2000 epochs (RMSE = 0.68 & R^2 = 0.97). These models capture both short-term variations and seasonal trends well (Figure 6b). The better performance of the LSTM for O3C_1 may be attributed to its simpler seasonal pattern compared to O3D_1. In the latter case, the deformation values were accurately predicted up to 150 days.

Table 1. *Models' performance metric for extensometer O3D_1 - Sequence Length = 100 & 200 across different epochs – Approach 1*

Epochs		MAE	RMSE	R-squared		MAE	RMSE	R-squared
50	Sequence Length = 100	3.305548	4.829045	0.370398	Sequence Length = 200	3.62967	5.314661	0.258326
80		3.450185	4.712311	0.400469		3.291272	4.775588	0.401154
100		3.120594	4.853092	0.364112		4.06606	5.8735	0.094151
200		3.214835	4.789904	0.380563		3.995137	5.841641	0.103952
500		2.519091	3.755772	0.619161		2.875817	4.220704	0.532231
1000		2.246045	3.259181	0.713212		2.99983	4.366276	0.499408
2000		4.87496	7.037257	-0.337058		4.116649	5.925414	0.078067

Table 2. *Models' performance metric for extensometer O3C_1 - Sequence Length = 100 & 200 across different epochs – Approach 1*

Epochs		MAE	RMSE	R-squared		MAE	RMSE	R-squared
50	Sequence Length = 100	0.980458	1.244236	0.904605	Sequence Length = 200	0.777990	0.927724	0.948959
80		0.756322	0.917841	0.948089		0.691296	0.856750	0.956470
100		0.633632	0.805933	0.959976		0.766386	0.902866	0.951657
200		0.805255	0.926715	0.947081		0.901370	1.201832	0.914341
500		0.404251	0.527602	0.982847		1.044013	1.149308	0.921665
1000		0.661128	0.867526	0.953625		0.652032	0.910955	0.950787
2000		0.740649	0.924701	0.947311		0.518556	0.679804	0.972594

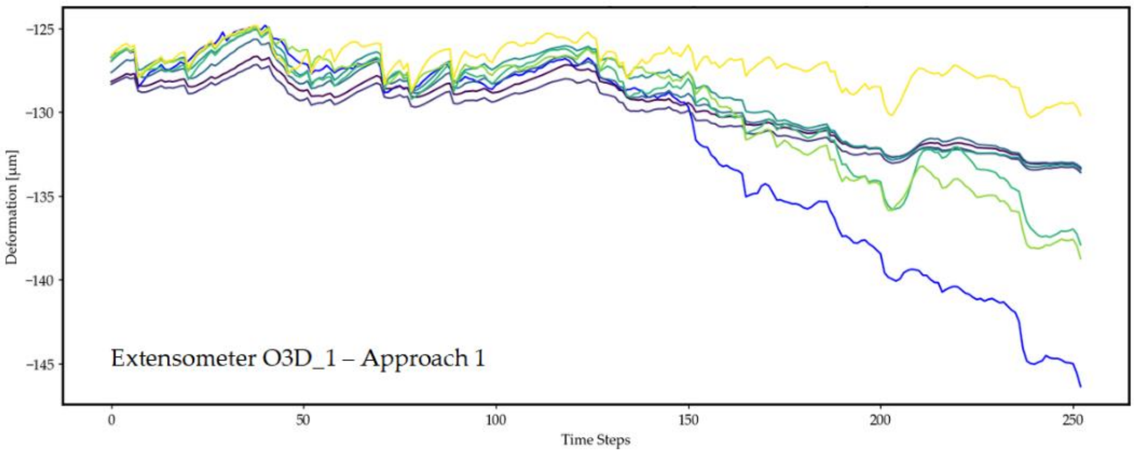

(a)

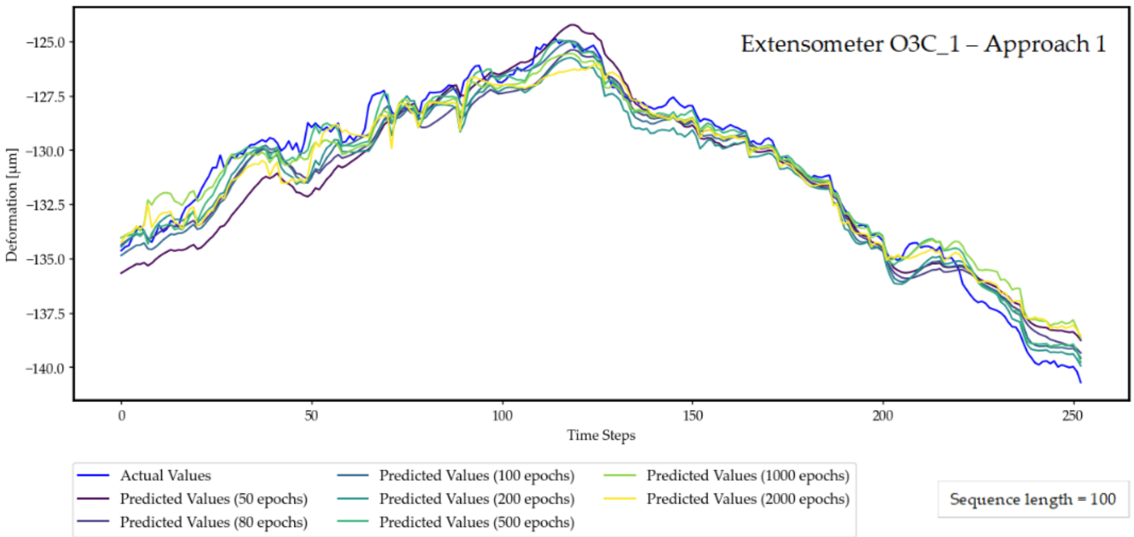

(b)

Figure 6. *Actual deformation values (blue) vs Predicted values for extensometer (a) O3D_1 and (b) O3C_1 with Sequence Length = 100 at Different Epochs – Approach 1*

Approach 2 – Retainment of the initial start-up phase

For the 2nd approach, the initial start-up phase is retained. After the removal of the fibre-optic system creep, a residual creep of the calcarenite pillars in the range of 20 μm over 4 years is obtained (Procedure A). The models' performance metrics are demonstrated in Table 3, while the predictions based on each model are presented in Figure 7a. As can be seen from the predictions, even though the log fit was removed, the model still struggles to effectively and accurately capture the deformations related to seasonality at the end of the test dataset. The same problem is seen during Procedure B, where the raw data from the extensometer, including the initial period, is fed into the LSTM without fitting a logarithmic curve (Figure 7b). In this case, the predictions are even worse compared to the previous methods.

Table 3. *Models' performance metric for extensometer O3D_1 - Sequence Length = 100 across different epochs for residual deformation – Approach 2 / Procedure A & B*

		Approach 2 / Procedure A				**Approach 2 / Procedure B**		
Epochs		**MAE**	**RMSE**	**R-squared**		**MAE**	**RMSE**	**R-squared**
50	Sequence Length = 100	0.868497	1.483057	0.931639	Sequence Length = 100	3.171623	4.373384	0.613013
80		1.032271	1.602657	0.920168		2.630001	3.48056	0.754891
100		1.033019	1.680293	0.912246		3.60344	4.920088	0.510214
200		0.821911	1.212075	0.954338		1.783001	2.554225	0.867998
500		0.707378	1.075797	0.964029		1.613145	2.342939	0.888934
1000		0.774209	1.238759	0.952305		1.911247	2.87948	0.83224
2000		1.80688	2.660377	0.780021		1.31533	1.919608	0.925443

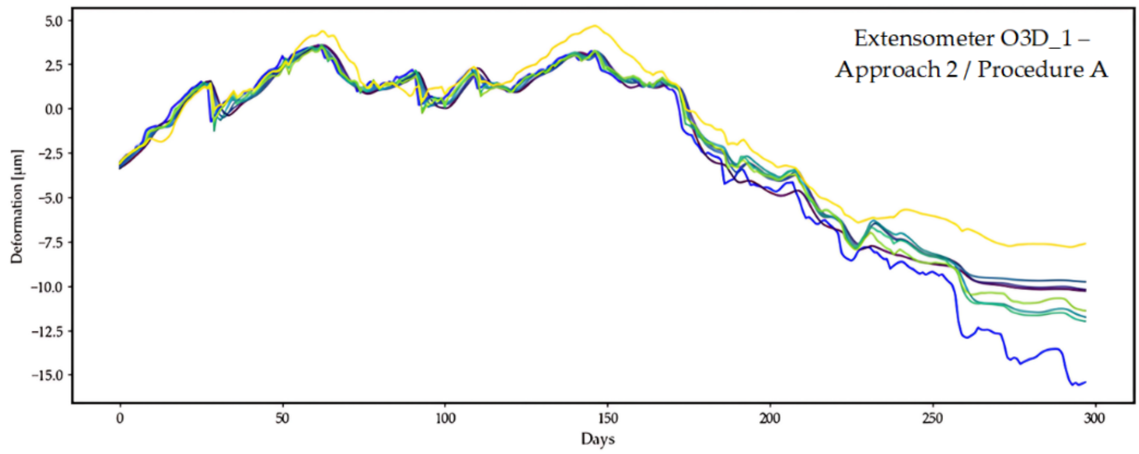

(a)

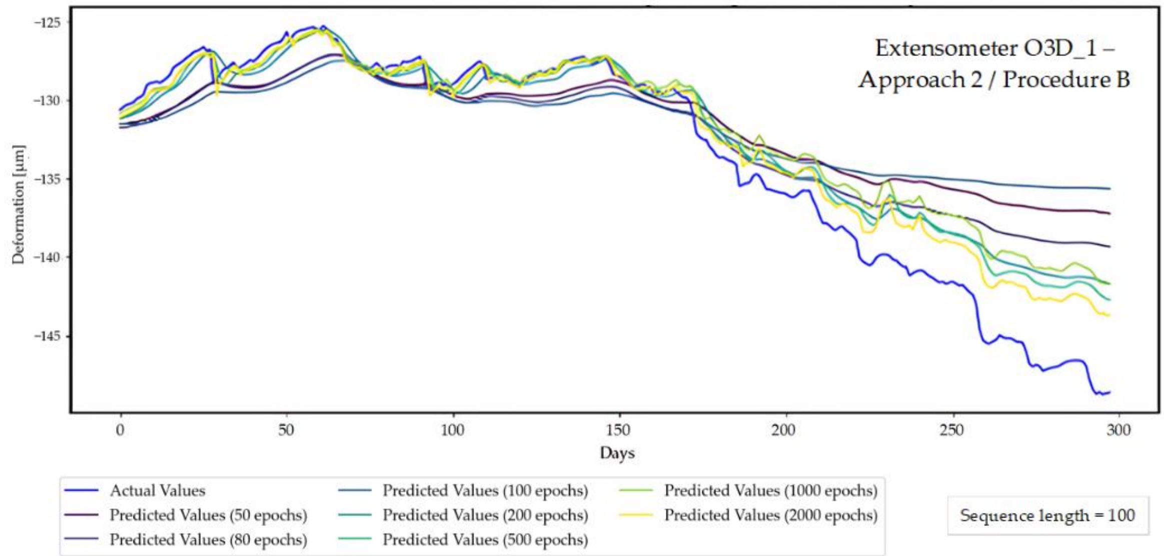

(b)

Figure 7. *Actual deformation values (blue) vs Predicted values for extensometer O3D_1 with Sequence Length = 100 at Different Epochs for (a) the residual deformation after the removal of the system creep (Approach 2 / Procedure A) and (b) for the raw dataset (Approach 2 / Procedure B)*

DISCUSSIONS

The LSTM approach, which was used to model creep deformation values from extensometers, demonstrated varying levels of effectiveness depending on the configuration of sequence lengths and epochs. As shown in Figure 8, the implementation of the first approach for extensometer O3D_1 reveals that the LSTM model struggles to accurately capture the underlying seasonal trends, particularly when dealing with longer sequence lengths, where the predictions tend to diverge from actual values. This issue was more pronounced in extensometers with complex deformation behaviours, where the model either overfitted or failed to generalise well beyond a certain number of epochs.

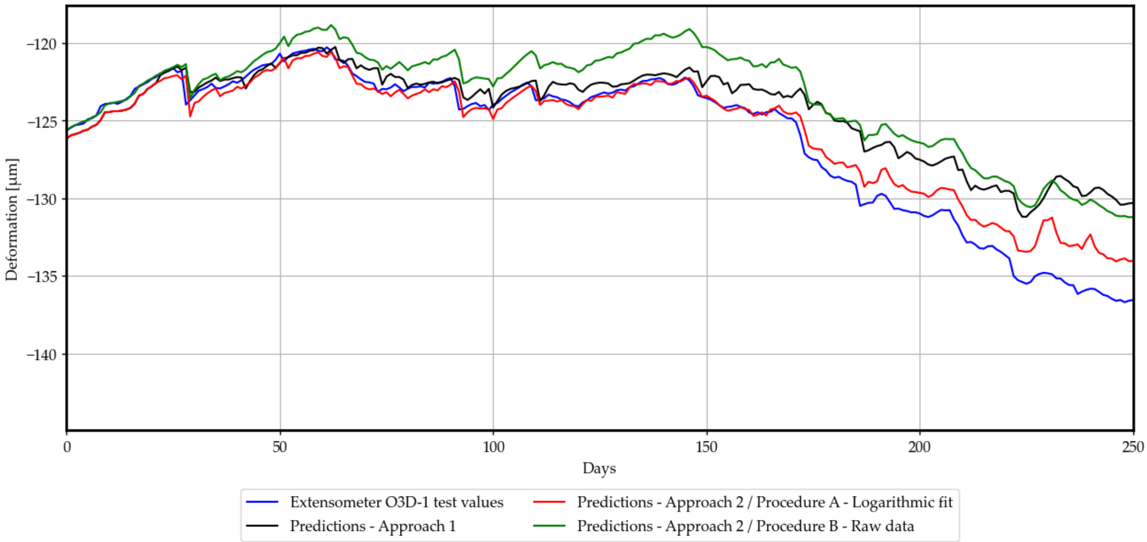

Figure 8. *Actual deformation values (blue) vs Best predictions for each Approach & Procedure for extensometer O3D_1*

When applying Procedure A for the second approach, the results demonstrated that fitting a logarithmic curve to the initial data effectively isolated the true creep behaviour of the limestone pillars, leading to more accurate predictions. In contrast, when applying Procedure B, where the initial startup phase was not removed or corrected and the raw dataset was fed directly into the LSTM model, the performance was the worst compared to all the other predictions.

When comparing all the predictions, the 2nd approach – Procedure A, which involved fitting a logarithmic curve to the initial data and removing the system-related creep, generally outperformed all the other approaches that either removed the initial start-up phase (Approach 1) or did not apply any correction to that phase (Approach 2 – Procedure B). This suggests that the logarithmic correction effectively mitigates the influence of the system-related part, allowing the LSTM model to focus on the true creep. Nonetheless, it should be emphasised that Approach 2 – Procedure A was implemented under the assumption that there is creep in the fibre optic system that is highly responsible for the deformation pattern. Whether that is the case is still to be directly examined.

Finally, it should be emphasized that the logarithmic fitting interpretation is specific to the monitoring conditions and instrumentation used in this study and that it remains an assumption, which requires further investigation and validation. Therefore, the applicability of the aforementioned method to other sites cannot be assumed a priori and should only be considered after verifying that similar system-related behaviour is present in the data.

CONCLUSIONS

In this study, the long-term creep behaviour of calcarenite mine pillars in the Valkenburggroeve is examined using four years of fibre optic monitoring data and LSTM neural networks. The LSTM models performed well in predicting short-term deformations. However, they faced challenges in capturing long-term seasonal patterns and often showed signs of overfitting with longer sequences. To address inconsistencies in the monitoring data, such as those related to the sensor relaxation or installation effects, a logarithmic correction was applied. This methodology effectively separated system-related creep from the true deformation of the pillars and significantly improved model accuracy and alignment with the observed time-dependent creep behaviour. However, the exact contribution of system-related creep remains uncertain and should be further investigated to validate the correction's assumptions.

The evaluation metrics used (MAE, RMSE, and R^2) complemented each other in evaluating the LSTM models. MAE showed the average prediction error in practical units, while RMSE emphasised larger deviations and model robustness. R^2 measured how well the models captured variance in the data. Together, they provided a balanced assessment of accuracy and reliability.

Future work could involve implementing more advanced architectures, such as xLSTM, to capture long-term dependencies better (Beck et al., 2024), or Physics-Informed LSTM (Phy-LSTM) to embed known physical creep behaviours into the learning process (Chen et al., 2024). Additionally, explainability tools such as SHAP values (Hu et al., 2023; Lundberg & Lee, 2017) could be employed to better understand the influence of each factor (temperature, precipitation, and pillar dimensions) on the pillar's deformation patterns, especially in the context of climate change.

ACKNOWLEDGEMENTS

The authors would like to express their gratitude to Fugro and the Municipality of Valkenburg for providing access to the monitoring datasets, as well as to Jacquo Silvertant, Hans Redder, and Edo Noordermeer, for their valuable contributions and support throughout this study.

REFERENCES

Beck, M., Pöppel, K., Spanring, M., Auer, A., Prudnikova, O., Kopp, M., Klambauer, G., Brandstetter, J., & Hochreiter, S. (2024). *xLSTM: Extended Long Short-Term Memory*. https://arxiv.org/abs/2405.04517v1

Bekendam, R. F. (1998). *Pillar stability and large-scale collapse of abandoned room and pillar limestone mines in South-Limburg, the Netherlands* [Doctoral Thesis, Delft University of Technology]. http://resolver.tudelft.nl/uuid:bfe483a5-312e-4213-ab45-1e75a147b1f2

Bekendam, R. F. (2008). *INVENTARISATIE STABILITEIT EN MILIEUONVRIENDELIJKE SITUATIES IN DE GEMEENTEGROEVE EN DE MONSTERGROT*.

Bekendam, R. F. (2019). *Voorlopige grenswaardes meetsysteem Gemeentegroeve en Sibbergroeve*.

Chen, X.-X., Zhang, P., & Yin, Z.-Y. (2024). Physics-Informed neural network solver for numerical analysis in geoengineering. *Georisk: Assessment and Management of Risk for Engineered Systems and Geohazards*, *18*(1), 33–51. https://doi.org/10.1080/17499518.2024.2315301

Felder, W., & Bosch, P. (2000). *Krijt van Zuid-Limburg*. TNO.

Franqueira, M. F. (2020). *Contribution to the geomechanical stability analysis of a marble underground exploitation using rockfill* [Master'sThesis].

He, Y., & Chen, Q. (2023a). Construction and Application of LSTM-Based Prediction Model for Tunnel Surrounding Rock Deformation. *Sustainability*, *15*(8), 6877. https://doi.org/10.3390/su15086877

He, Y., & Chen, Q. (2023b). Construction and Application of LSTM-Based Prediction Model for Tunnel Surrounding Rock Deformation. *Sustainability*, *15*(8), 6877. https://doi.org/10.3390/su15086877

Hu, L., Corporate, W., Risk, M., & Fargo, W. (2023). *Computing SHAP Efficiently Using Model Structure Information*. https://doi.org/https://doi.org/10.48550/arXiv.2309.02417

Leontjeva, A., & Kuzovkin, I. (2016). Combining Static and Dynamic Features for Multivariate Sequence Classification. *IEEE International Conference on Data Science and Advanced Analytics (DSAA)*.

Lundberg, S. M., & Lee, S. I. (2017). A Unified Approach to Interpreting Model Predictions. *Advances in Neural Information Processing Systems*, *2017-December*, 4766–4775. https://doi.org/https://doi.org/10.48550/arXiv.1705.07874

Noordermeer, E., Bekendam, R., Beers, K., Nachenius, A., & Karabacak, D. (2023). Monitoring the rock mechanical safety of underground limestone quarries using fibre optic sensing technology. In W. Schubert & A. Kluckner (Eds.), *Proceedings of the ISRM 15th International Congress on Rock Mechanics and Rock Engineering & 72nd Geomechanics Colloquium – Challenges in Rock Mechanics and Rock Engineering* (pp. 1400–1405). Austrian Society for Geomechanics. https://eposter.at/ISRM2023/data/PDF/1306.pdf

Seo, S., & Chung, M. (2022). Evaluation of Applicability of 1D-CNN and LSTM to Predict Horizontal Displacement of Retaining Wall According to Excavation Work. *International Journal of Advanced Computer Science and Applications*, *13*(2). https://doi.org/10.14569/IJACSA.2022.0130210

Van Paassen, L. A., Van Loosdrecht, M. C. M., Van Den Eijnden, A. P., Mulder, A., Verwaal, W., Ngan-Tillard, D. J. M., Harkes, M. P., & Bekendam, R. F. (2008). Reinforcement of calcarenite room and pillar mines by microbially induced carbonate precipitation. *EuroEngeo 2008, Madrid: Escuela de Ingenieria de Obras Publicas Madrid, Spain*.

Xie, P., Zhou, A., & Chai, B. (2019). The Application of Long Short-Term Memory(LSTM) Method on Displacement Prediction of Multifactor-Induced Landslides. *IEEE Access*, *7*, 54305–54311. https://doi.org/10.1109/ACCESS.2019.2912419